IEEE Photonics Journal
An IEEE Photonics Society Publication

Refractive Index Fiber Laser Sensor by Using Tunable Filter Based on No-Core Fiber

Volume 8, Number 5, October 2016

Junfa Zhao
Juan Wang
Cheng Zhang
Cuijuan Guo
Hua Bai
Wei Xu
Liying Chen
Changyun Miao

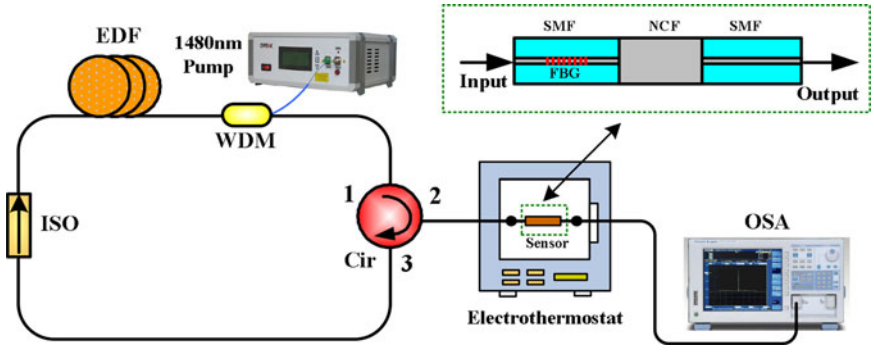

DOI: 10.1109/JPHOT.2016.2609598
1943-0655 © 2016 IEEE

Refractive Index Fiber Laser Sensor by Using Tunable Filter Based on No-Core Fiber

Junfa Zhao,[1,2] Juan Wang,[1,2] Cheng Zhang,[1,2] Cuijuan Guo,[1,2] Hua Bai,[1,2] Wei Xu,[1,2] Liying Chen,[1,2] and Changyun Miao[1,2]

[1]Tianjin Key Laboratory of Optoelectronic Detection Technology and Systems, Tianjin Polytechnic University, Tianjin 300387, China
[2]School of Electronics and Information Engineering, Tianjin Polytechnic University, Tianjin 300387, China

DOI:10.1109/JPHOT.2016.2609598

Manuscript received August 1, 2016; revised September 6, 2016; accepted September 12, 2016. Date of publication September 14, 2016; date of current version September 30, 2016. This work was supported in part by the National Natural Science Foundation of China under Grant 61201106, Grant 61307094, and Grant 61501324; in part by Tianjin Research Program of Application Foundation and Advanced Technology under Grant 14JCQNJC01800 and Grant 15JCYBJC16300; and in part by Tianjin City High School Science and Technology Fund Planning Project under Grant 20140713. Corresponding author: C. Guo (e-mail: guocuijuan@tjpu.edu.cn).

Abstract: A novel refractive index fiber laser sensor based on a fiber Bragg grating (FBG) integrated with a section of no-core fiber (NCF) is proposed and experimentally demonstrated. The oscillating wavelength of the fiber laser is only decided by the central wavelength of the FBG that is insensitive to the surrounding refractive index (SRI). However, the output power of the fiber laser varies with the SRI because the laser output is filtered by the edge of the bandpass filter (BPF) formed by the multimode interference (MMI) effect in the NCF, which is sensitive to the SRI. By measuring the variation of the output power, a cost-effective power detection RI sensor could be realized. The fiber laser sensor has a linear relationship with SRI and a sensitivity of 113.73 dB/RIU in the RI range of 1.333–1.4076.

Index Terms: Fiber laser sensor, no-core fiber, refractive index sensing.

1. Introduction

Refractive index (RI) measurements play an important role in chemical and biological industries. Owing to their intrinsic advantages such as high sensitivity, miniaturize size, immunity to electromagnetic interference and low cost, fiber optic RI sensors have been widely studied and realized in many different ways, such as fiber gratings [1]–[3], Mach-Zehnder interferometers (MZIs) [4]–[6], Fabry-Perot interferometers (FPIs) [7]–[9], and multimode interferometers [10]–[12]. Recently, multimode interferometers based on no-core fiber (NCF) have been deeply investigated for RI measurement [13], [14]. The structure is constructed by using a section of NCF spliced between two single mode fibers (SMFs). The NCF is a kind of multimode fiber (MMF) which uses surrounding media as its cladding. Therefore, multimode interference (MMI) effect in the NCF is easily influenced by the surrounding refractive index (SRI). This kind of sensor is sensitive to the SRI.

For most of the wavelength encoded RI sensing system based on broadband light source, the resolution is relatively low because the 3 dB bandwidth of the transmission spectrum is large. In

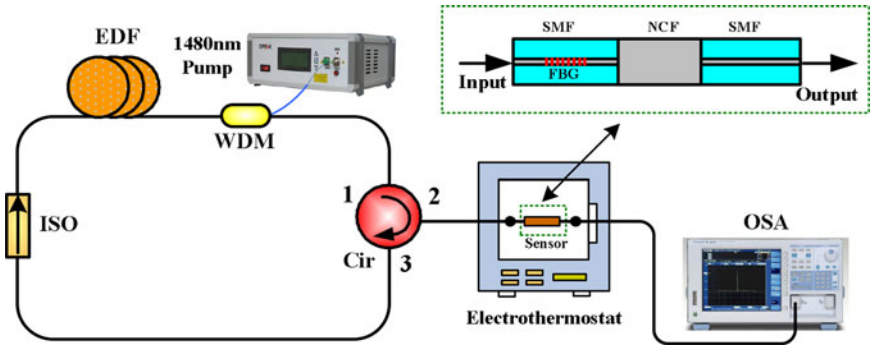

Fig. 1. Experiment setup of the proposed laser sensor.

order to improve the measurement accuracy, fiber laser sensors based on SMF-NCF-SMF (SNS) structure were proposed [15]–[17]. It is worth noting that the demodulation system of the wavelength encoded sensing system is complicated and expensive. It often needs an optical spectrum analyzer (OSA) to discriminate the wavelength shift, which should be restrained in practical applications. Assisted by the reflection of fiber Bragg gratings (FBG), cost-effective power detection RI sensors could be implemented by measuring the variation of the reflective optical power at the Bragg wavelength [18], [19].

In this paper, we proposed and demonstrated a RI fiber laser sensor based on a FBG integrated with a section of NCF. The SNS structure in the laser sensor is only used as the sensing head, which is different from previous reports using the SNS structure not only as the filter but also as the sensing head [15]–[17]. The oscillating wavelength is determined by the central wavelength of the FBG, and then the laser output is filtered by the edge of the bandpass filter (BPF) based on the SNS structure. A cost-effective power detection RI sensor could be realized through measuring the variation of the output power. The laser output is stable, which has a higher optical signal-to-noise ratio (OSNR) and narrower 3 dB bandwidth. The linearity of the sensor is good enough during the measurement range. Moreover, surrounding temperature measurement can be realized by monitoring the peak wavelength of the laser output.

2. Principle and Experiment Setup

The schematic diagram of the proposed refractive index fiber laser sensor is depicted in Fig. 1. The sensing head fixed straightly along the platform of an electrothermostat is composed of a FBG cascaded with a BPF based on SNS structure. The SNS structure is fusion spliced with the AUTO MODE in the splicer menu, which is easy to be fabricated by a common commercial fiber fusion splicer (FSM-60s, Fujikura). It should be pointed out that although the fabrication of the SNS structure is easy, it still needs precisely controlling the NCF length and carefully fusion splicing procedures to ensure the transmission spectrum of the BPF. A 8 m long erbium-doped fiber (EDF, GP980) with an absorption coefficient of 12.26 dB/m near 1530 nm is used as the gain medium, which is pumped by a 1480 nm pump laser diode with a maximum output power of 250 mW through a 1480/1550 nm wavelength division multiplexer (WDM). A 3-port optical circulator (Cir) is used to reflect the lasing light into the ring cavity and a dual-stage optical isolator (ISO) is inserted to provide unidirectional oscillating. In addition to be used as the filter of the fiber laser, the FBG plays a major role in probing surrounding temperature, and therefore, the distance between the FBG and NCF is limited to a few millimeters to ensure the FBG and NCF in the same measurement environment. The total cavity length is about 20 m. The central wavelength of the FBG is insensitive to the SRI [20], but it is sensitive to the surrounding temperature, and therefore, the peak wavelength will keep constant at a fixed surrounding temperature. The laser output from the right end of the FBG is filtered by the edge of the transmission spectrum of the BPF which is sensitive to the SRI, and then monitored by an OSA (AQ6370B). This way, the wavelength shift influenced by the SRI is converted

to the output power variation of the laser sensor. The SRI can be measured based on the output power of the laser sensor.

The BPF is formed by MMI effect in the NCF. When the fusion process is ideal, only the linearly polarization LP_{0m} modes are excited and transmitted in NCF. The input electric field of NCF can be expressed as [21]

$$E(r,0) = \sum_{m=1}^{M} c_m E_m(r) \tag{1}$$

where $E_m(r)$ is the field profile of LP_{0m} mode, and c_m is the excitation coefficient of LP_{0m} mode, which can be expressed by

$$c_m = \frac{\int_0^\infty E(r,0)E_m(r)rdr}{\int_0^\infty E_m(r)E_m(r)rdr} \tag{2}$$

Then, after propagating a distance z in NCF, the field distribution can be calculated by

$$E(r,z) = \sum_{m=1}^{M} c_m E_m(r)\exp(j\beta_m z) \tag{3}$$

where β_m is the propagation constant of the LP_{0m} mode. From (3), it can be seen that the NCF section field is influenced by the parameters r and z. Therefore, the diameter and length of the NCF will influence the interference within the NCF. The effective RI of the cladding of the NCF will be changed as the RI of the surrounding media varied. As a result, the interference spectrum will be changed with the SRI. To study the field distribution along the NCF, a numerical simulation based on the beam propagation method and parameters used in our experiment was carried out [22]. The core refractive index of the NCF is 1.44 and diameter D is 125 μm. The surrounding air acts as the cladding of the NCF which has a refractive index of 1.0. The input SMF has a core and cladding diameter of 8.2 μm and 125 μm, and the corresponding refractive indices are 1.4682 and 1.4628, respectively. Owing to the self-imaging effect, the energies of the excited high-order modes periodically gather and become a peak in the propagation direction. Fig. 2(a) shows the field distribution along the NCF at the wavelength of 1525 nm and Fig. 2(b) shows the corresponding normalized optical intensity variation. It can be clearly seen the fourth self-image is 59 mm at the input wavelength of 1525 nm. In order to achieve moderate spectrum and minimum insertion loss [16], [23], 59 mm NCF was selected to be used in our experiments. The black spectrum in Fig. 3 shows the measured transmission spectrum of the BPF with 59 mm NCF in air. The peak wavelength is about 1525 nm, which is consistent with the input wavelength of the simulation. Based on the MMI theory, the peak wavelength of the BPF can be calculated by

$$\lambda_0 = \frac{4n_{NCF}D_{NCF}^2}{L} \tag{4}$$

where L is the length of the NCF, and n_{NCF} and D_{NCF} are the effective RI and diameter of the NCF. When the SRI of the NCF increases, the difference between the core and cladding is reduced, which leads to the increase of n_{NCF} and D_{NCF}. According to Eq. (4) the peak wavelength should shift to longer wavelength. The red and blue spectrum in Fig. 3 show the measured transmission spectra of the BPF when the NCF was immersed in deionized water and glycerol solution with 1.4076 RI, respectively. It can be seen that the shape of the transmission spectra almost remain unchanged, only the peak wavelength of the spectra shift from 1536 nm to 1548 nm, which is in good agreement with the theoretical prediction.

The central wavelength of the FBG has a direct influence on the SRI measurement. In order to have a linear response of the SRI, it should be located on the relatively smooth edge of the BPF and must be always on one side of the peak wavelength of the BPF during the measurement range. Based on the measured transmission spectra at different SRIs, as shown in Fig. 3, the central wavelength of the FBG used in our experiment is selected at 1550.19 nm. The inset of Fig. 3 shows

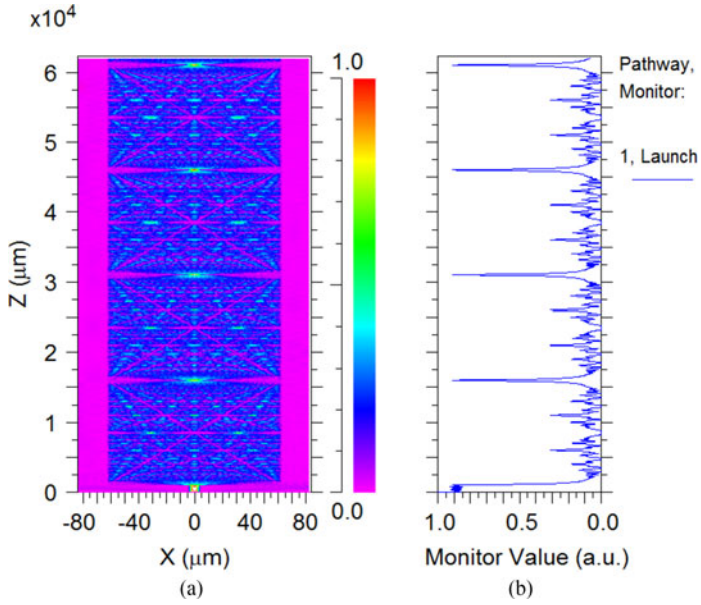

Fig. 2. (a) Field distribution and (b) normalized optical intensity varies along the NCF at wavelength of 1525 nm.

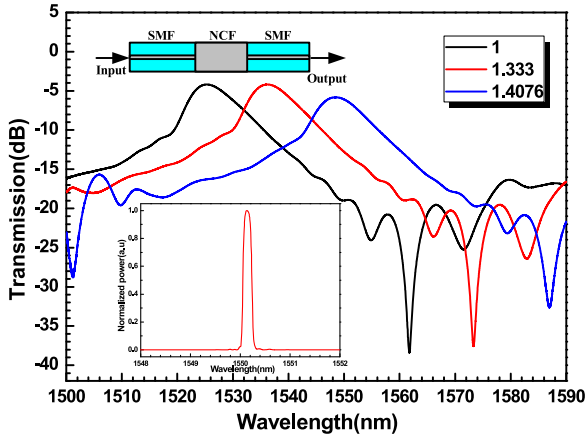

Fig. 3. Transmission spectra of the SNS structure at different SRIs. (Inset) Normalized reflection spectrum of the selected FBG.

the normalized reflection spectrum of the selected FBG. The FBG has a 3 dB bandwidth of 0.18 nm and a reflectivity of 93.87%.

3. Experiment Results and Discussions

Fig. 4 shows the output spectrum of the laser sensor when the sensing head is in air. The lasing wavelength is 1550.19 nm which is consistent with the central wavelength of the FBG. The laser spectrum has a narrower linewidth about 0.04 nm, and the OSNR is higher than 55 dB. The inset shows the stability of the laser output during half an hour with an interval of two minutes. The measured power fluctuations are less than 0.08 dB. Glycerol solutions with different concentration were prepared as the liquid samples for measuring the SRI response of the laser sensor. The RIs of the samples were calibrated by an Abbe refractometer and vary from 1.333 to 1.4076.

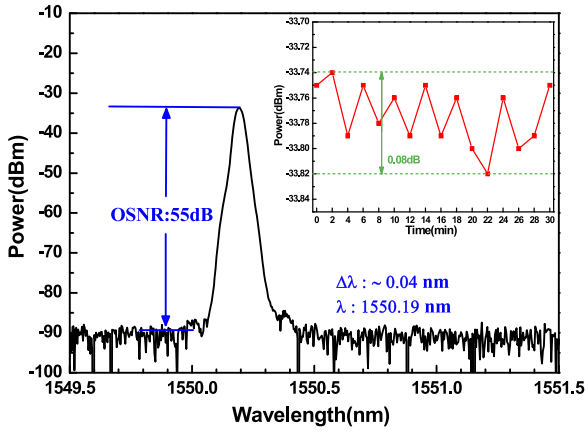

Fig. 4. Output spectrum of the laser sensor when the sensing head is in air. (Inset) Stability of the laser sensor.

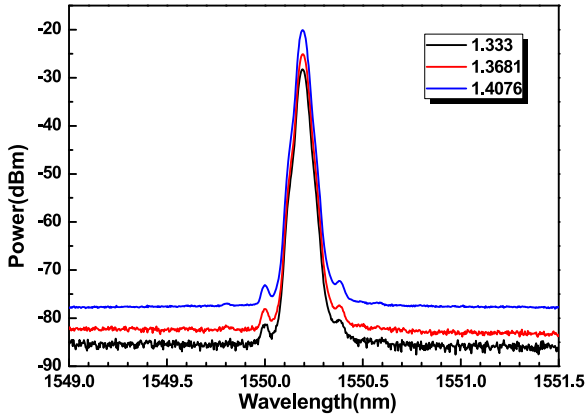

Fig. 5. Output spectra of the laser sensor at surrounding RI of 1.333, 1.3681, and 1.4076.

The surrounding temperature of the sensing head was kept at 25 °C, and the 1480 nm pump power was fixed at 250 mW. During the measurement, the sensing head was totally immersed in liquid samples and the sensing head was repeatedly cleaned by deionized water and dried in air after each measurement. Fig. 5 shows the selected output spectra of the laser sensor at the SRI of 1.333, 1.3681 and 1.4076. The peak wavelength is fixed at 1550.19 nm, and the output power increases with the refractive indices. As the SRI increases, the transmission spectrum of the BPF has a red shift to longer wavelength, which in turn reduces the insertion loss of the FBG location and thus makes the output power increased. Compared with the RI sensor based on reflection spectrum of the FBG [19], the fiber laser sensor has the advantages of higher output power, narrower linewidth and higher OSNR. The measurement accuracy can be significantly improved by measuring the peak power of the laser sensor. Furthermore, the output power can also be measured via a cost-effective power meter. The relationship between the SRI and the output power is depicted in Fig. 6 when the SRI changes from 1.333 to 1.4076. The linear fit has an R^2 value of 0.994 and indicates that the RI sensitivity is 113.73 dB/RIU. It worth noting that the RI measurement range and sensitivity are determined by the transmission spectrum of the BPF and the central wavelength of the FBG. During the measurement range, the peak wavelength of the BPF should always locate on the left side of the FBG to get a linear response. In order to expand the measurement range, the central wavelength of the FBG should be moved to longer wavelength, but it cannot exceed the linearity

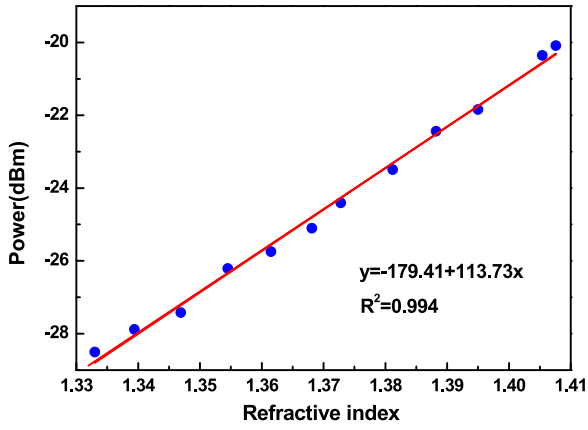

Fig. 6. Output power of the laser sensor as a function of the SRI.

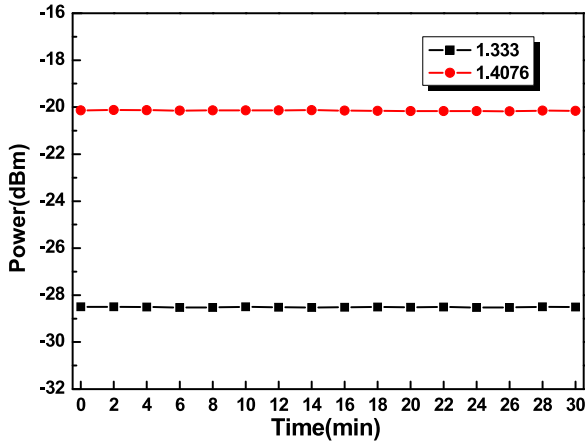

Fig. 7. Output power stability of the laser sensor at SRI of 1.333 and 1.4076.

range of the BPF fringe. Furthermore, the sensing sensitivity is directly related to the wavelength shift of the BPF and the slope of the BPF fringe. At a certain RI range, the BPF based on thinner NCF has a larger wavelength shift [24], which can lead to more power variation. Another effective way is to double the length of the NCF used in the SNS structure because the doubled length of the NCF can narrow the bandwidth of the BPF, which leads to the steep BPF fringe. The steep BPF fringe can induce more power variation at a certain RI range, which effectively improve the sensing sensitivity, but it should be noted that the steep BPF fringe limits the measurement range.

The output power stability of the laser sensor has a direct influence on the measurement accuracy of the sensor. In order to evaluate the measurement error, the output powers were recorded every two minutes within half an hour when the sensing head was immersed in deionized water and glycerol solution with 1.4076 RI, respectively. During the measurement time, the maximum power fluctuations are 0.03 dB and 0.06 dB, as shown in Fig. 7, corresponding the maximum RI measurement error of 5.27×10^{-4} RIU. That means the laser sensor has a stable output and the measurement error can be neglected.

Thermal effect will also result in the spectrum drift, and so temperature variation will induce the cross sensitivity. In order to characterize the temperature response of the sensor, the electrothermostat was adjusted from 30 °C to 80 °C with a step of 10 °C, and the sensing head was fully exposed in air. The output peak wavelength and power were recorded at different temperature, as shown in

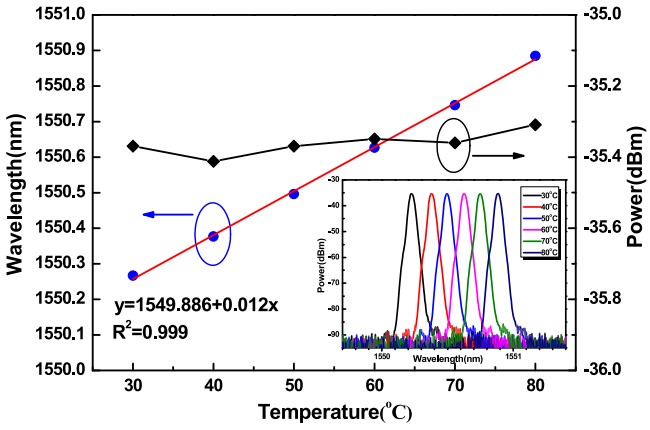

Fig. 8. Temperature sensitivity and peak power fluctuation of the laser sensor. (Inset) Output spectra at different temperature.

Fig. 8. The peak wavelength increases linearly with the temperature with a sensitivity of 12 pm/°C, while the maximum peak-to-peak power fluctuations is only 0.1 dB. The corresponding maximum RI measurement error is about 8.79×10^{-4} RIU, which indicates the temperature variation does not have significant influence on the RI measurement. This phenomenon is attributed to the fact that the transmission spectrum of the BPF has the same wavelength shift direction with the FBG [25]. The relative wavelength shift caused by temperature variations can be written as $\Delta\lambda/\lambda = (\alpha_{NCF} + \xi)\Delta T$, where α_{NCF} is the coefficient of thermal expansion, and ξ is the thermo-optic coefficient of the NCF material. It is obvious that an increase in temperature will cause the transmission spectrum of the BPF to shift to longer wavelengths. The transmission spectrum shift then compensates the power fluctuation caused by the wavelength shift of the FBG. The proposed sensor has potential application in temperature-immune RI measurement. Moreover, the oscillating wavelength of the laser sensor is only determined by the central wavelength of the FBG, which is sensitive to the surrounding temperature. Therefore, temperature measurement can be realized by detecting the peak wavelength of the laser output.

4. Conclusion

In conclusion, we have proposed and demonstrated a novel RI fiber laser sensor based on FBG integrated with NCF structure. The oscillating wavelength of the fiber laser keeps constant at the fixed pump power and surrounding temperature because the FBG is insensitive to the SRI. However, the ultimate output power varies with the SRI due to the edge filter through the BPF based on SNS structure which is sensitive to the SRI. This converts the SRI information into the variation of the output power. The fiber laser sensor shows a linear sensitivity of 113.73 dB/RIU in the RI range of $1.333-1.4076$. The fiber laser sensor has a stable output and the maximum RI measurement error is only 5.27×10^{-4} RIU. Thermal effect has little effect on the measurement of RI due to the wavelength shift compensation of the SNS structure. Moreover, by discriminating the peak wavelength of the laser output, temperature measurement can be realized.

References

[1] W. Liang, Y. Y. Huang, Y. Xu, R. K. Lee, and A. Yariv, "Highly sensitive fiber Bragg grating refractive index sensors," *Appl. Phys. Lett.*, vol. 86, no. 15, Apr. 2005, Art. no. 151122.

[2] N. Chen, B. Yun, and Y. Cui, "Cladding mode resonances of etch-eroded fiber Bragg grating for ambient refractive index sensing," *Appl. Phys. Lett.*, vol. 88, no. 13, Mar. 2006, Art. no. 133902.

[3] C. Guan, X. Tian, S. Li, X. Zhong, J. Shi, and L. Yuan, "Long period fiber grating and high sensitivity refractive index sensor based on hollow eccentric optical fiber," *Sens. Actuators B, Chem.*, vol. 188, pp. 768–771, Aug. 2013.
[4] K. Ni, X. Dong, C. Chan, T. Li, L. Hu, and W. Qian, "Miniature refractometer based on Mach–Zehnder interferometer with waist-enlarged fusion bitaper," *Opt. Commun.*, vol. 292, pp. 84–86, Apr. 2013.
[5] X. Liu, Y. Zhao, R. Lv, and Q. Wang, "High sensitivity balloon-like interferometer for refractive index and temperature measurement," *IEEE Photon. Technol. Lett.*, vol. 28, no. 13, pp. 1485–1488, Jul. 2016.
[6] X. Zhang, Z. Liu, L. Xie, and W. Peng, "Refractive index sensor based on fiber ring laser," *IEEE Photon. Technol. Lett.*, vol. 28, no. 4, pp. 524–527, Feb. 2016.
[7] C. Liao, T. Hu, and D. Wang, "Optical fiber Fabry–Perot interferometer cavity fabricated by femtosecond laser micromachining and fusion splicing for refractive index sensing," *Opt. Exp.*, vol. 20, no. 20, pp. 22813–22818, Sep. 2012.
[8] D. Wu, T. Zhu, G. Y. Wang, J. Y. Fu, X. G. Lin, and G. L. Gou, "Intrinsic fiber-optic Fabry–Perot interferometer based on arc discharge and single-mode fiber," *Appl. Opt.*, vol. 52, no. 12, pp. 2670–2675, Apr. 2013.
[9] T. Wang and M. Wang, "Fabry–Pérot fiber sensor for simultaneous measurement of refractive index and temperature based on an in-fiber ellipsoidal cavity," *IEEE Photon. Technol. Lett.*, vol. 24, no. 19, pp. 1733–1736, Oct. 2012.
[10] Y. Zhao, L. Cai, and X. G. Li, "High sensitive modal interferometer for temperature and refractive index measurement," *IEEE Photon. Technol. Lett.*, vol. 27, no. 12, pp. 1341–1344, Jun. 2015.
[11] Y. Chen *et al.*, "A hybrid multimode interference structure-based refractive index and temperature fiber sensor," *IEEE Sensors J.*, vol. 16, no. 2, pp. 331–335, Jan. 2016.
[12] X. Zhou, K. Chen, X. Mao, P. Wei, and Q. Yu, "A reflective fiber-optic refractive index sensor based on multimode interference in a coreless silica fiber," *Opt. Commun.*, vol. 340, pp. 50–55, Apr. 2015.
[13] L. Li, L. Xia, Y. Wuang, Y. Ran, C. Yang, and D. Liu, "Novel NCF-FBG interferometer for simultaneous measurement of refractive index and temperature," *IEEE Photon. Technol. Lett.*, vol. 24, no. 24, pp. 2268–2271, Dec. 2012.
[14] X. Liu, X. Zhang, Y. Liu, Z. Liu, and W. Peng, "Multi-point fiber-optic refractive index sensor by using coreless fibers," *Opt. Commun.*, vol. 365, pp. 168–172, Apr. 2016.
[15] Z. Liu, Z. Tan, B. Yin, Y. Bai, and S. Jian, "Refractive index sensing characterization of a singlemode-claddingless-singlemode fiber structure based fiber ring cavity laser," *Opt. Exp.*, vol. 22, no. 5, pp. 5037–5042, Mar. 2014.
[16] L. Man, Y. Qi, Z. Kang, Y. Bai, and S. Jian, "Tunable fiber laser based on the refractive index characteristic of MMI effects," *Opt. Laser Technol.*, vol. 57, pp. 96–99, Apr. 2014.
[17] Q. Meng, X. Dong, K. Ni, Y. Li, B. Xu, and Z. Chen, "Optical fiber laser salinity sensor based on multimode interference effect," *IEEE Sensors J.*, vol. 14, no. 6, pp. 1813–1816, Jun. 2014.
[18] Y. Ma *et al.*, "Reflective fiber-optic refractometer based on a thin-core fiber tailored Bragg grating reflection," *Opt. Lett.*, vol. 37, no. 3, pp. 323–325, Feb. 2012.
[19] M. Shao *et al.*, "Refractive index measurement based on fiber Bragg grating connected with a multimode fiber core," *Opt. Commun.*, vol. 51, pp. 70–74, Sep. 2015.
[20] T. Liu, Y. Chen, Q. Han, F. Liu, and Y. Yao, "Sensor based on macrobent fiber Bragg grating structure for simultaneous measurement of refractive index and temperature," *Appl. Opt.*, vol. 55, no. 4, pp. 795–791, Feb. 2016.
[21] Q. Wu *et al.*, "Fiber refractometer based on a fiber Bragg grating and single-mode-multimode-single-mode fiber structure," *Opt. Lett.*, vol. 36, no. 12, pp. 2197–2199, Jun. 2011.
[22] X. Bai, H. Wang, S. Wang, S. Pu, and X. Zeng, "Refractive index sensing characteristic of single-modemultimode-single-mode fiber structure based on self-imaging effect," *Opt. Eng.*, vol. 54, no. 10, Oct. 2015, Art. no. 106103.
[23] J. E. Antonio-Lopez et, J. J. Sanchez-Mondragon, P. LiKamWa, and D. A. May-Arrioja, "Fiber-optic sensor for liquid level measurement," *Opt. Lett.*, vol. 36, no. 17, pp. 3425–3427, Sep. 2011.
[24] Q. Wang, Y. Semenova, P. Wang, and G. Farrell, "High sensitivity SMS fiber structure based refractermeter-analysis and experiment," *Opt. Exp.*, vol. 19, no. 9, pp. 7937–7944, Apr. 2011.
[25] J. Huang, X. Lan, A. Kaur, H. Wang, L. Yuan, and H. Xiao, "Temperature compensated refractometer based on a cascaded SMS/LPFG fiber structure," *Sens. Actuators B, Chem.*, vol. 198, pp. 384–387, Jul. 2014.